2023 62nd IEEE Conference on Decision and Control (CDC)
December 13-15, 2023. Marina Bay Sands, Singapore

Stability Analysis for a Platoon of Vehicles with Reaction-Time Delay

Shima Sadat Mousavi†, Somayeh Bahrami‡, and Anastasios Kouvelas†

***Abstract*— This paper explores collective dynamics in a group of multiple homogeneous vehicles on a ring-road using the Optimal Velocity Model (OVM). To account for real-world traffic scenarios, driver reaction time is incorporated as a time-delay system. Analyzing stability, we initially focus on the equilibrium motion regime, where vehicles maintain uniform speed and spacing. This is achieved through linearization and examining the impact of model parameters. Subsequently, we extend our analysis to the full nonlinear model, determining the equilibrium's region of attraction by solving Linear Matrix Inequalities (LMIs) and estimating ellipsoids.**

I. Introduction

In recent decades, the transportation industry has seen significant changes driven by automation technologies like automated vehicles and infrastructure improvements [1]. As the industry shifts from human-driven to fully automated vehicles, it presents new challenges. Therefore, there's a pressing need to investigate mixed traffic systems, which encompass both human-driven and automated vehicles, as demonstrated in recent studies [2].

Several experimental studies confirm the emergence of stop-and-go waves in traffic flow. For example, a practical experiment on a single-lane ring-road [3] observed stop-and-go waves triggered by a platoon of human-driven vehicles (HDVs). These waves propagate upstream, disrupting uniform flow and causing phantom traffic jams. This instability has been studied from macroscopic [4], cellular automaton [5], and microscopic [6] perspectives. Nonlinear wave amplification factors include stochastic driver behavior, lane changes, road features, and ramps. Recent studies have explored how connected and automated vehicles (CAVs) can mitigate traffic waves [7]–[9]. In a field experiment ([10]), a single CAV in a platoon on a circular roadway effectively dissipated waves. Theoretical analysis in [11] examined the capability of a solitary CAV to regulate traffic flow on a ring-roadway. Theoretical research ([12]–[14]) has shown a single CAV's ability to control traffic flow on a ring-roadway.

CAVs have proven effective in traffic control, but their precise role in stabilizing traffic when integrated with HDVs remains unclear. Thus, there's a pressing need to advance traffic flow stability research. In this study, we analyze uniform flow equilibrium stability within the Optimal Velocity Model (OVM) framework to enhance traffic control methods. It's important to note that many investigations of mixed traffic depend on linearizing nonlinear dynamics around the equilibrium flow. Recently, in [15], [16], a nonlinear stability analysis was presented for a platoon of vehicles following the OVM. However, this analysis used simplified dynamics that omitted consideration of drivers' reaction time. The significance of including the time-delay arising from drivers' reactions was initially introduced in [17] and further underscored by [18]. It's important to note that stability analysis in systems with time-delay is generally more intricate than in systems without any delay.

This paper aims to overcome classical linear stability analysis limitations by delving into traffic flow's nonlinear dynamics and stability. To do so, we extend the findings of [15] by incorporating a time-delay system to represent drivers' reaction time. Our analysis begins with linearizing the nonlinear model around the uniform flow equilibrium, assessing its stability using the Routh–Hurwitz stability criterion [19]. However, linearization confines the stability examination to a local vicinity of the equilibrium, limiting insights into trajectories of the original nonlinear model when far from this point. In the latter part of this paper, we shift focus to the nonlinear model, aiming to establish its region of attraction through ellipsoidal approximations. Using this approach and solving appropriate Linear Matrix Inequalities (LMIs), we determine a portion of the state space where trajectories of the nonlinear model will inevitably converge to the equilibrium point.

Notation: The set of real numbers is denoted by $\mathbb{R}$. The transpose of matrix M is represented by M^T. For a vector v, v_i is its ith entry. $\mathbf{1}_n$ denotes the vector of all ones in $\mathbb{R}^n$. We denote the identity matrix by I. We use also the notation $He(A) = A + A^T$.

II. Mathematical model of a platoon on a ring

In this section, we model the car-following behaviour of a platoon of n HDVs. The vehicles are assumed to move along a single-lane ring-road of length L. The position and the velocity of the ith vehicle are, respectively, denoted by p_i and v_i. The spacing between vehicle i and the preceding vehicle $i-1$ is represented by s_i (i.e., $s_i = p_{i-1} - p_i$).

The Optimal Velocity Model for n vehicles, as introduced by Bando et al. [6], can be described as follows:

$$\begin{aligned} \dot{s}_i(t) &= v_{i-1}(t) - v_i(t), \\ \dot{v}_i(t) &= b\Big(V_{\text{opt}}(s_i(t-\tau)) - v_i(t-\tau)\Big), \end{aligned} \tag{1}$$

where b represents a constant that reflects the sensitivity of the driver, and τ is the human reaction time delay. Moreover,

*This work was supported in part by the Swiss National Science Foundation (SNSF) under the project RECCE "Realtime traffic estimation and control in a connected environment", contract No. 200021-188622.

†The authors are with the Institute for Transport Planning and Systems, ETH Zurich, Switzerland, {shimaossadat.mousavi, anastasios.kouvelas}@ivt.baug.ethz.ch

‡The author is with the Department of Electrical Engineering, Razi University, Kermanshah, Iran, s.bahrami@razi.ac.ir

the optimal velocity function is given by:

$$V_{\text{opt}}(s) = v_{\max}\frac{\tanh(s-l-s_{\text{safe}})+\tanh(l+s_{\text{safe}})}{1+\tanh(l+s_{\text{safe}})}, \quad (2)$$

where $v_{\max}$ represents the maximum speed of the vehicle, l denotes the length of the vehicle, and s_{safe} refers to the safe spacing required between two adjacent vehicles i and $i-1$ to prevent any potential collision. We let $d_0 := l + s_{\text{safe}}$.

We first calculate the equilibrium points of the dynamics (1). Given the equilibrium speed v^*, the equilibrium spacing s^* can be obtained by solving the equation $V_{\text{opt}}(s^*) = v^*$. Since at the equilibrium speed, all the vehicles keep the same distance, one can write $s^* = L/n := d$.

Now, for $i = 1, \dots, n$, by defining the state error as $x_i = \begin{bmatrix}\tilde{s}_i & \tilde{v}_i\end{bmatrix}^T = \begin{bmatrix}s_i - s^* & v_i - v^*\end{bmatrix}^T$, we can rewrite the dynamics of HDV i as

$$\begin{aligned}\dot{\tilde{s}}_i(t) &= \tilde{v}_{i-1}(t) - \tilde{v}_i(t),\\ \dot{\tilde{v}}_i(t) &= b\Big(v_{\max}\frac{\tanh\left(\tilde{s}_i(t-\tau)+d-d_0\right)-\tanh(d-d_0)}{1+\tanh(d_0)}\\ &\quad - \tilde{v}_i(t-\tau)\Big),\end{aligned} \quad (3)$$

where $i-1 = n$ if $i = 1$. Now, let us define $x_i^T = \begin{bmatrix}\tilde{s}_i & \tilde{v}_i\end{bmatrix}$. The aggregated state vector for all vehicles can also be defined as $x = \begin{bmatrix}x_1^T & \dots & x_n^T\end{bmatrix}^T \in \mathbb{R}^{2n}$. Since the vehicles move along a ring-road, we have $\sum_{i=1}^n \tilde{s}_i = 0$. Thus, $\tilde{s}_n = -\sum_{i=1}^{n-1}\tilde{s}_i$. The reduced state vector is defined as

$$\bar{x} = \begin{bmatrix}x_1^T & \dots & x_{n-1}^T & \tilde{v}_n\end{bmatrix}^T \in \mathbb{R}^{2n-1}. \quad (4)$$

III. Stability Analysis of Linearized System

In this section, we present initial findings based on a linear analysis conducted around the zero equilibrium point. In light of (3), the linearized model of the platoon around the new equilibrium, that is, the origin, is compactly described as

$$\dot{x}(t) = Ax(t) + A_\tau x(t-\tau), \quad (5)$$

where

$$A = \begin{bmatrix}A_1 & 0 & 0 & \dots & A_2\\ A_2 & A_1 & 0 & \dots & 0\\ \vdots & \ddots & \ddots & \ddots & \vdots\\ 0 & \dots & 0 & A_2 & A_1\end{bmatrix},\ A_\tau = \begin{bmatrix}A_{\tau 1} & 0 & \dots & 0\\ 0 & A_{\tau 1} & \dots & 0\\ \vdots & \ddots & \ddots & \vdots\\ 0 & \dots & 0 & A_{\tau 1}\end{bmatrix}, \quad (6)$$

with $A_1 = \begin{bmatrix}0 & -1\\ 0 & 0\end{bmatrix}$, $A_2 = \begin{bmatrix}0 & 1\\ 0 & 0\end{bmatrix}$, $A_{\tau 1} = \begin{bmatrix}0 & 0\\ \gamma & -b\end{bmatrix}$, and

$$\gamma = bv_{\max}\frac{\operatorname{sech}^2(d-d_0)}{1+\tanh(d_0)}.$$

Moreover, the reduced-order model can be described as:

$$\dot{\bar{x}}(t) = \bar{A}\bar{x}(t) + \bar{A}_\tau \bar{x}(t-\tau), \quad (7)$$

where

$$\bar{A} = \begin{bmatrix}A_1 & 0 & 0 & \dots & \bar{A}_2\\ A_2 & A_1 & 0 & \dots & 0\\ \vdots & \ddots & \ddots & \ddots & \vdots\\ 0 & \dots & A_2 & A_1 & 0\\ 0 & \dots & 0 & 0 & 0\end{bmatrix},\ \bar{A}_\tau = \begin{bmatrix}A_{\tau 1} & 0 & \dots & 0\\ 0 & A_{\tau 1} & \dots & 0\\ \vdots & \ddots & \ddots & \vdots\\ 0 & \dots & A_{\tau 1} & 0\\ A_{\tau 2} & \dots & A_{\tau 2} & -b\end{bmatrix}, \quad (8)$$

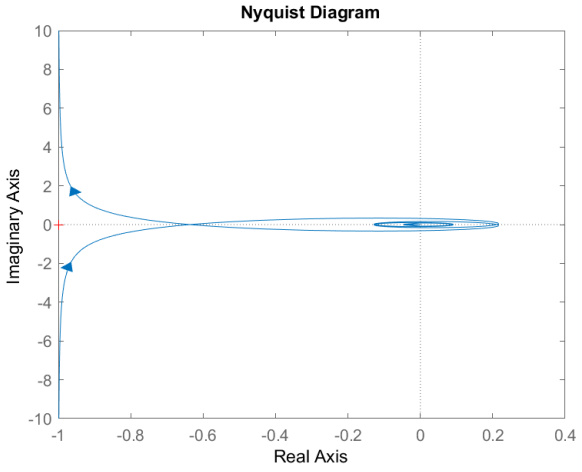

Fig. 1. Nyquist diagram of the transfer function $g(s) = \frac{be^{-\tau s}}{s}$.

with $\bar{A}_2 = [1 \quad 0]^T$, $A_{\tau 2} = [-\gamma \quad 0]$.

Now, for $k = 1, \dots, n-1$, let us define:

$$\mathcal{Q}(s) := s + be^{-\tau s},\ \ \mathcal{P}_k(s) := s^2 + be^{-\tau s}s + \gamma(1-\omega^k)e^{-\tau s}, \quad (9)$$

where $\omega = \exp\left(\frac{2\pi j}{n}\right)$. Moreover, $\mathcal{P}(s)$ is defined as

$$\mathcal{P}(s) := \mathcal{Q}(s)\prod_{k=1}^{n-1}\mathcal{P}_k(s). \quad (10)$$

The next result provide a stability condition for system (7).

Proposition 1: System (7) is stable if and only if $\max\{\Re(s) : \mathcal{P}(s) = 0\} < 0$.

Proof. Let $B = A + A_\tau e^{-\tau s}$ (resp., $\bar{B} = \bar{A} + \bar{A}_\tau e^{-\tau s}$). Moreover, define $\bar{B}_1 = \begin{bmatrix}0 & -1\\ \gamma e^{-\tau s} & -be^{-\tau s}\end{bmatrix}^T$, $B_2 = \begin{bmatrix}0 & 1\\ 0 & 0\end{bmatrix}$. Let Λ and $\bar{\Lambda}$ be , respectively, the set of eigenvalues of B and $\bar{B}$. Then, $\Lambda = \bar{\Lambda}\cup\{0\}$. Moreover, since B is a circulant matrix, Λ can be easily found [20]. Then, by defining $\omega = \exp\left(\frac{2\pi j}{n}\right)$, the characteristic polynomial of $\bar{B}$ takes the form

$$\begin{aligned}\mathbf{det}(sI - \bar{B}) &= \prod_{k=0}^{n-1}\mathbf{det}(sI - B_1 - B_2\omega^k)\\ &= (s+be^{-\tau s})\prod_{k=1}^{n-1}\left(s^2 + be^{-\tau s}s + \gamma(1-\omega^k)e^{-\tau s}\right) = \mathcal{P}(s).\end{aligned}$$

Thus, from Theorem 1.5 in [21], the result is verified. ■

Theorem 1: If system (7) is stable, $\tau < \frac{\pi}{2b}$ should hold.

Proof. If system (7) is stable, $\max\{\Re(s) : \mathcal{Q}(s) = s + be^{-\tau s} = 0\} < 0$. Now, consider the transfer function $g(s) = \frac{be^{-\tau s}}{s}$, whose Nyquist diagram is shown in Fig. 1. One can see that $\mathcal{Q}(s)$ has no root in the right half-plane if and only if the point -1 lies outside the encirclement of the Nyquist diagram of $g(s)$. Let $r^* + j0$ be the closest point of the Nyquist diagram to -1. Then, $r^* = -\frac{2\tau b}{\pi}$. Therefore, if system (7) is stable, $r^* > -1$, implying that $\tau < \frac{\pi}{2b}$. ■

Now, let us consider the following Pade approximation of degree one for the time-delay term $e^{-\tau\lambda}$ as $e^{-\tau s} \approx \frac{2-\tau s}{2+\tau s}$.

Then, $\mathcal{P}_k(s)$ in (9) can be approximated as the following polynomial with complex coefficients:

$$\mathcal{P}_k(s) \approx \bar{\mathcal{P}}_k(s) = \tau s^3 + a^1 s^2 + (a_k^2 + j b_k^2)s + a_k^3 + j b_k^3, \quad (11)$$

where

$$\begin{aligned} a^1 &= 2 - b\tau, \\ a_k^2 &= 2b - \gamma\tau\big(1 - \cos(2\pi k/n)\big), \\ b_k^2 &= \gamma\tau \sin(2\pi k/n), \\ a_k^3 &= 2\gamma\big(1 - \cos(2\pi k/n)\big), \\ b_k^3 &= -2\gamma \sin(2\pi k/n). \end{aligned} \quad (12)$$

Now, let us define the following parameters:

$$\begin{array}{lll} m_k^1 = -\tau b_k^2, & m_k^2 = a^1 a_k^2 - \tau a_k^3, & m_k^3 = a^1 b_k^3, \\ p_k^1 = a^1 m_k^2 + m_k^1 b_k^2, & p_k^2 = a^1 m_k^3 - m_k^1 a_k^3, & \\ q_k^1 = p_k^1 b_k^2 - a^1 p_k^2, & q_k^2 = p_k^1 a_k^3, & \\ r_k = p_k^1 q_k^2 + p_k^2 q_k^1. & & \end{array}$$

By the next result, one can check whether $\bar{\mathcal{P}}_k(s)$ in (11) is Hurwitz or not.

Theorem 2: For $k = 1, \ldots, n-1$, the polynomial $\bar{\mathcal{P}}_k(s)$ is stable if and only if all the parameters a^1, p_k^1, and r_k are positive.

Proof. For the polynomial $\bar{\mathcal{P}}(s)$ with complex coefficients, we form a generalized Routh array as follows [22]:

s^3	τ	0	a_k^2	b_k^3
s^2	a^1	b_k^2	a_k^3	
	m_k^1	m_k^2	m_k^3	
s^1	p_k^1	p_k^2		
	q_k^1	q_k^2		
s^0	r_k			

Therefore, $\bar{\mathcal{P}}(s)$ is stable if and only if τ, a^1, p_k^1, and r_k which are on the first column have the same sign. ■

Corollary 1: A system with dynamics (7) and $\tau = 0$ is stable if and only if

$$\frac{\gamma}{b^2} < \frac{1}{1 + \cos\left(\frac{2\pi}{n}\right)}. \quad (13)$$

Proof. According to Proposition 1, the system's stability is contingent upon the stability of all the roots of $\mathcal{P}(s)$. Theorems 1 and 2 indicate that the system's stability is established if and only if $r_k > 0$ for $k = 1, \ldots, n-1$. This requirement is met if $b^2 > \gamma\Big(1 - cos\big(\frac{2\pi k}{n}\big)\Big)$ for all $1 \le k \le n-1$. The most stringent restriction is encountered when $k = 2$, resulting in (13). ■

Example 1: Consider a platoon of $n = 22$ vehicles, moving along a ring-road of $L = 220\ m$. Thus, $d = L/n = 10\ m$. Furthermore, let us set $d_0 := l + s_{\text{safe}} = 10\ m$, $b = 10\ s^{-1}$, and $v_{\max} = 5\ m/s$. Applying Theorems 1 and 2, we can calculate the maximum delay ensuring the stability of $\mathcal{Q}(s)$ and $\bar{\mathcal{P}}_k(s)$ for $k = 1, \ldots, n-1$, which is found to be $\tau = 0.117\ s$. Figs. 2 (a), (b), and (c), respectively, display the stability regions in the (γ, b)-plane, $(v_{\max}, b)$-plane, and $(d - d_0, b)$-plane. In these figure, the corresponding values of the parameters γ, $v_{\max}$, $d - d_0$, b, and τ that ensure the stability of the approximation of the linearized system (7) are shown. The color-bar on the right-hand side is used to associate different colors with various values of the delay τ. We observe that the boundary between the stable and the unstable region (which is represented by the white region) can be approximated by setting the inequality in (13) to equality. To illustrate, in Figs. 2 (a,b), the boundary is approximated by the equations $\gamma \approx 0.51 b^2$ and $\gamma \approx 1.02 b$, respectively, which can also be derived from (13). Additionally, (13) indicates that the boundary in Fig. 2 (c) is described by the equation $b = 4.9\text{sech}^2(d - d_0)$, which can be verified through the figure.

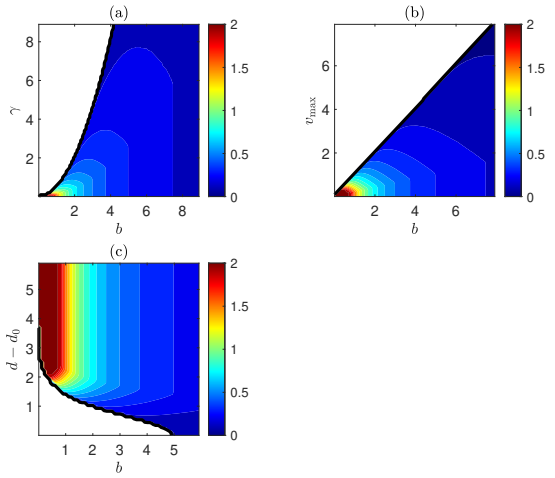

Fig. 2. Stability of the system with dynamics (7) in the (a) (γ, b)-plane, (b) $(v_{\max}, b)$-plane, (c) $(d - d_0, b)$-plane, when changing the amount of the delay τ (c.f. color bar on the right).

IV. Region of Attraction

The results in Section III are based on a linearized model of the nonlinear system (3), which inherently provides local insights. However, they do not provide information about the region of attraction (ROA) of the origin under real nonlinear dynamics. To address this limitation, the following section shifts its focus to the nonlinear system (3) itself and strives to estimate the ROA of the origin.

We rewrite the nonlinear dynamic equations (3) as

$$\begin{aligned} \dot{\bar{x}} = \bar{A}\bar{x} + \mathcal{A}_\tau \bar{x}(t-\tau) \\ + B\Big(\tanh\big(K\bar{x}(t-\tau) + \tilde{d}\big) - \tanh\big(\tilde{d}\big)\Big), \end{aligned} \quad (14)$$

where $\bar{x}$ and $\bar{A}$ are defined in (4) and (8), respectively. Moreover, we have $\tilde{d} = (d - d_0)\mathbf{1}_n$, $B = \dfrac{bv_{\max}}{1 + \tanh(d_0)}\text{diag}\{B_1, \ldots, B_1, 1\} \in \mathbb{R}^{2n-1 \times n}$, and

$$\mathcal{A}_\tau = \begin{bmatrix} \mathcal{A}_{\tau 1} & 0 & \cdots & 0 \\ 0 & \mathcal{A}_{\tau 1} & \cdots & 0 \\ \vdots & \ddots & \ddots & \vdots \\ 0 & \cdots & \mathcal{A}_{\tau 1} & 0 \\ 0 & \cdots & 0 & -b \end{bmatrix}, \; K = \begin{bmatrix} K_1 & 0 & 0 & \cdots & 0 \\ 0 & K_1 & 0 & \cdots & 0 \\ \vdots & \ddots & \ddots & \ddots & \vdots \\ K_2 & \cdots & K_2 & K_2 & 0 \end{bmatrix}, \quad (15)$$

with $B_1 = [0 \quad 1]^T$, $\mathcal{A}_{\tau 1} = \begin{bmatrix} 0 & 0 \\ 0 & -b \end{bmatrix}$, $K_1 = [1 \quad 0]$, $K_2 = [-1 \quad 0]$. It is clear that $K\bar{x} = \tilde{s} = \begin{bmatrix} \tilde{s}_1 & \dots & \tilde{s}_n \end{bmatrix}^T \in \mathbb{R}^n$, where $\tilde{s}_n = -\sum_{i=1}^{n-1} \tilde{s}_i$. In the following, we obtain an estimation of the ROA of the equilibrium point of the nonlinear system (14). It is straightforward to show that $\bar{x} = 0$ is an equilibrium for (14). By the following Lemma, we bound the nonlinear function $\tanh(\cdot)$ by a local sector.

Lemma 1: [23] Let $\bar{z}, \underline{z} \in \mathbb{R}$, $z^* \in [\underline{z}, \bar{z}]$, and

$$\beta(\underline{z}, \bar{z}) := \min \Big\{ \frac{\tanh(\bar{z}) - \tanh(z^*)}{\bar{z} - z^*}, \frac{\tanh(z^*) - \tanh(\underline{z})}{z^* - \underline{z}} \Big\},$$

where $\beta < 1$. Then, for all $\underline{z} \leq z \leq \bar{z}$, the function $\tanh(\cdot)$ is bounded by the local sector $[\beta(\underline{z}, \bar{z}), 1]$ with the center $\big(z^*, \tanh(z^*)\big)$. In other words, defining $\Delta\mathcal{F} = \tanh(z) - \tanh(z^*)$ and $\Delta Z = z - z^*$, we can write

$$\Big(\Delta\mathcal{F} - \beta(\underline{z}, \bar{z})\Delta Z\Big)\Big(\Delta Z - \Delta\mathcal{F}\Big) \geq 0.$$

Note that the vector-valued function $\tanh : \mathbb{R}^n \to \mathbb{R}^n$ is appeared in the right hand side of (14), and we need to extend the result of Lemma 1 to this vector-valued function. Let $\mathcal{B} \in \mathbb{R}^n$ and $\underline{z}, \bar{z} \in \mathbb{R}^n$, where for all $i \in \{1, 2, ..., n\}$, $\mathcal{B}_i := \beta(\underline{z}_i, \bar{z}_i)$. Then, based on Lemma 1, it is straightforward to show that for all $\underline{z} \leq z \leq \bar{z}$ and $\underline{z} \leq z^* \leq \bar{z}$, the function $\tanh(\cdot)$ holds the following inequality

$$\psi(z, z^*)^T \Upsilon^T \Omega(\alpha) \Upsilon \psi(z, z^*) \geq 0, \tag{16}$$

where

$$\psi(z, z^*) := \begin{bmatrix} z - z^* \\ \tanh(z) - \tanh(z^*) \end{bmatrix}, \quad \Upsilon := \begin{bmatrix} I_n & -I_n \\ -\text{diag}\{\mathcal{B}\} & I_n \end{bmatrix}, \tag{17}$$

$$\Omega(\alpha) := \begin{bmatrix} 0 & \text{diag}(\alpha) \\ \text{diag}(\alpha) & 0 \end{bmatrix}, \quad \alpha \in \mathbb{R}^n_{\geq 0}. \tag{18}$$

Theorem 3: Consider the system (14). Let $z = K\bar{x}(t - \tau) + \tilde{d}$, $z^* = \tilde{d}$, $\bar{z} \geq z^*$ and $\underline{z} = 2z^* - \bar{z}$. If there exist the positive definite matrices P, Q and R, a vector $\alpha \geq 0$, and the positive scalar q that for maximum allowed delay $\bar{\tau}$ satisfy the LMIs (20) and (21), then the set

$$\mathcal{S}(P, q) := \Big\{ \bar{x} \in \mathbb{R}^{2n-1} : \bar{x}^T P \bar{x} \leq q^{-1} \Big\} \tag{19}$$

is an estimation of the ROA of the origin. In the LMI (21), the notation K_i refers to the i^{th} row of the matrix K.

Proof. First, consider the LMI (21). Using the Schur complement [24], this LMI is equivalent to

$$K_i P^{-1} K_i^T \leq q(\bar{z}_i - z_i^*)^2, \tag{22}$$

for $i = 1, ..., n$. Based on Lemma 1 in [25], we can conclude

$$\mathcal{S}(P, q) \subseteq \Big\{ x : \underline{z} - z^* \leq K\bar{x} \leq \bar{z} - z^* \Big\}.$$

Defining $z - z^* = K\bar{x}$, we have

$$\mathcal{S}(P, q) \subseteq \Big\{ x : \underline{z} \leq z \leq \bar{z} \Big\}.$$

Therefore, feasibility of (21) yields that if $\bar{x} \in \mathcal{S}(P, q)$, then $\underline{z} \leq z \leq \bar{z}$, and hence the inequality (16) is valid.

Now, using the Newton-Leibniz model transformation [26], one can write $\bar{x}(t - \tau) = \bar{x}(t) - \int_{t-\tau}^{t} \dot{\bar{x}}(\zeta) d\zeta$. Then, the time-delayed system (14) can be expressed as

$$\dot{\bar{x}} = \bar{A}\bar{x} + \mathcal{A}_\tau \bar{x}(t) - \mathcal{A}_\tau \int_{t-\tau}^{t} \dot{\bar{x}}(\zeta) d\zeta + B\Big(\tanh\big(z\big) - \tanh\big(z^*\big) \Big). \tag{23}$$

Now, consider the following Lyapunov-Krasovskii functional

$$V = \bar{x}^T P \bar{x} + \int_{t-\tau}^{t} \bar{x}^\top(\zeta) Q \bar{x}(\zeta) d\zeta + \int_{-\tau}^{0} \int_{t+\zeta}^{t} \dot{\bar{x}}^\top(\eta) R \dot{\bar{x}}(\eta) d\eta d\zeta, \tag{24}$$

where $P, Q, R \succeq 0$. Computing the derivative of V along the trajectories of the system (23) yields

$$\begin{aligned} \dot{V} = {} & \bar{x}^T \Big(\big(\bar{A} + \mathcal{A}_\tau\big)^T P + P\big(\bar{A} + \mathcal{A}_\tau\big) + Q \Big) \bar{x} \\ & - 2\bar{x}^T P \mathcal{A}_\tau \int_{t-\tau}^{t} \dot{\bar{x}}(\zeta) d\zeta + 2\bar{x}^T P B \Big(\tanh\big(z\big) - \tanh\big(z^*\big) \Big) \\ & - \bar{x}^T(t - \tau) Q \bar{x}(t - \tau) + \tau \dot{\bar{x}}^T R \dot{\bar{x}} - \int_{t-\tau}^{t} \dot{\bar{x}}^\top(\zeta) R \dot{\bar{x}}(\zeta) d\zeta. \end{aligned} \tag{25}$$

Since $R \succeq$, using the Young inequality [27], the cross-term $-2\bar{x}^T P \mathcal{A}_\tau \int_{t-\tau}^{t} \dot{\bar{x}}(\zeta) d\zeta$ can be upper bounded easily as

$$-2\bar{x}^T P \mathcal{A}_\tau \int_{t-\tau}^{t} \dot{\bar{x}}(\zeta) d\zeta \leq \bar{\tau} \bar{x}^T P \mathcal{A}_\tau R^{-1} \mathcal{A}_\tau^T P \bar{x} + \int_{t-\tau}^{t} \dot{\bar{x}}^\top(\zeta) R \dot{\bar{x}}(\zeta) d\zeta. \tag{26}$$

Substituting this bound in $\dot{V}$, we get

$$\begin{aligned} \dot{V} \leq {} & \bar{x}^T \Big(\big(\bar{A} + \mathcal{A}_\tau\big)^T P + P\big(\bar{A} + \mathcal{A}_\tau\big) + Q \\ & + \bar{\tau} P \mathcal{A}_\tau R^{-1} \mathcal{A}_\tau^T P \Big) \bar{x} + 2\bar{x}^T P B \Big(\tanh\big(z\big) - \tanh\big(z^*\big) \Big) \\ & - \bar{x}^T(t - \tau) Q \bar{x}(t - \tau) + \tau \dot{\bar{x}}^T R \dot{\bar{x}}. \end{aligned} \tag{27}$$

Finally, expanding the term $\tau \dot{\bar{x}}^T R \dot{\bar{x}}$ yields

$$\dot{V} \leq \xi^T \Xi \xi, \tag{28}$$

where $\xi = \begin{bmatrix} \bar{x}^T & \bar{x}^T(t - \tau) & \Big(\tanh\big(z\big) - \tanh\big(z^*\big) \Big)^T \end{bmatrix}^T$, and Ξ is defined in (29). As well known, if $\dot{V}$ is negative, then the system (14) is stable. Furthermore, based on the Schur complement, the LMI (20) is equivalent to the matrix inequality (30). Obviously, (30) can be rewritten as

$$\Xi + \Gamma^T \Upsilon^T \Omega(\alpha) \Upsilon \Gamma < 0, \tag{31}$$

where Γ is

$$\Gamma = \begin{bmatrix} 0 & K & 0 \\ 0 & 0 & I_{2n-1} \end{bmatrix}, \tag{32}$$

and the matrices Υ and $\Omega(\alpha)$ are defined in (17) and (18). Now, by pre-and-post multiplying (31) by ξ^T and ξ, we have

$$\xi^T \Xi \xi + \xi^T \Gamma^T \Upsilon^T \Omega(\alpha) \Upsilon \Gamma \xi < 0. \tag{33}$$

$$\begin{bmatrix} He\big(P(\bar{A}+\mathcal{A}_\tau)\big)+Q+\bar{\tau}\bar{A}^T R\bar{A} & \bar{\tau}\bar{A}^T R\mathcal{A}_\tau & PB+\bar{\tau}\bar{A}^T RB & \bar{\tau}P\mathcal{A}_\tau \\ * & -Q+\bar{\tau}\mathcal{A}_\tau^T R\mathcal{A}_\tau-2K^T\text{diag}(\alpha)\text{diag}(\mathcal{B})K & \bar{\tau}\mathcal{A}_\tau^T RB+K^T\text{diag}(\alpha)+K^T\text{diag}(\alpha)\text{diag}(\mathcal{B}) & 0 \\ * & * & \bar{\tau}B^T RB-2\text{diag}(\alpha) & 0 \\ * & * & * & -\bar{\tau}R \end{bmatrix} \prec 0, \tag{20}$$

$$\begin{bmatrix} q(\bar{z}_i-z_i^*)^2 & K_i \\ K_i^T & P \end{bmatrix} \succeq 0, \quad i=1,...,n. \tag{21}$$

$$\Xi = \begin{bmatrix} He\big(P(\bar{A}+\mathcal{A}_\tau)\big)+Q+\bar{\tau}\bar{A}^T R\bar{A}+\bar{\tau}P\mathcal{A}_\tau R^{-1}\mathcal{A}_\tau^T P & \bar{\tau}\bar{A}^T R\mathcal{A}_\tau & PB+\bar{\tau}\bar{A}^T RB \\ * & -Q+\bar{\tau}\mathcal{A}_\tau^T R\mathcal{A}_\tau & \bar{\tau}\mathcal{A}_\tau^T RB \\ * & * & \bar{\tau}B^T RB \end{bmatrix}. \tag{29}$$

$$\begin{bmatrix} He\big(P(\bar{A}+\mathcal{A}_\tau)\big)+Q+\bar{\tau}\bar{A}^T R\bar{A}+\bar{\tau}P\mathcal{A}_\tau R^{-1}\mathcal{A}_\tau^T P & \bar{\tau}\bar{A}^T R\mathcal{A}_\tau & PB+\bar{\tau}\bar{A}^T RB \\ * & -Q+\bar{\tau}\mathcal{A}_\tau^T R\mathcal{A}_\tau-2K^T\text{diag}(\alpha)\text{diag}(\mathcal{B})K & \bar{\tau}\mathcal{A}_\tau^T RB+K^T\text{diag}(\alpha)+K^T\text{diag}(\alpha)\text{diag}(\mathcal{B}) \\ * & * & \bar{\tau}B^T RB-2\text{diag}(\alpha) \end{bmatrix} \prec 0. \tag{30}$$

It is straightforward to show that $\xi^T\Gamma^T=\psi(z,z^*)$, defined in (17). Therefore, the inequality (33) is rewritten as

$$\xi^T\Xi\xi+\psi(z,z^*)^T\Upsilon^T\Omega(\alpha)\Upsilon\psi(z,z^*)<0. \tag{34}$$

Considering (16), (28) and (34), it is obvious that $\dot{V}<0$, and thereby the proof is complete. ■

According to Theorem 3, an inner-approximation of the ROA of the system (14) can be obtained. This ROA is represented by an ellipsoid whose volume is influenced by the LMI variables P and q. In order to reduce the conservatism in the estimation of the ROA, a convex optimization problem can be solved to minimize the values of P and q. As q and the trace of P decrease, the volume of the ellipsoid increases, leading to a more accurate estimation of the ROA. Therefore, an optimal estimation of the ROA can be obtained by solving the following convex optimization problem:

$$\begin{aligned} &\text{minimize} \quad \text{trace}\ (P)+q, \\ &\text{subjuct to LMIs (20) and (21).} \end{aligned} \tag{35}$$

The inclusion $\mathcal{S}(P,q)\subseteq\left\{x:\underline{z}-z^*\leq K\bar{x}\leq\bar{z}-z^*\right\}$ indicates that the optimal estimation of the ROA, obtained by solving the optimization problem (35), is influenced by the value of $\bar{z}$. A larger value of $\bar{z}$ results in a wider ROA, but this also increases the difficulty of satisfying the LMI (21), to the point where it may become infeasible. Therefore, striking a balance between the size of the ROA and the feasibility of the optimization problem requires careful consideration of the value of $\bar{z}$.

Example 2: Similar to Example 1, we consider a platoon containing $n=22$ vehicles, moving along a ring-road with length $L=220\ m$. Choose the parameters of the system similar to Example 1, that is, $d=10\ m$, $d_0=10\ m$, $b=10\ s^{-1}$, $v_{\max}=5\ m/s$. As previously determined, with these parameter values, the maximum allowable delay for the system to remain stable is $\tau=0.117\ s$. In this case, as $z^*=\tilde{d}=d-d_0=0$, the local sector is centered at the origin $(0,0)$. The maximum feasible value of $\bar{z}$ for which the LMI (21) can be satisfied is $\bar{z}_i=0.5601$ for $i=1,...,n$. By solving the optimization problem (35), we obtain the optimal ellipsoidal ROA $\mathcal{S}(P,q)$, which is then plotted along with its intersections with the $(\tilde{s}_1,\tilde{s}_2)$ and $(\tilde{v}_1,\tilde{v}_2)$ planes in Figs. 3 (a,b). As shown, the red trajectory originates inside $\mathcal{S}(P,q)$, remains within it, and ultimately reaches the origin. However, as $\mathcal{S}(P,q)$ is an underestimate of the true ROA, some trajectories, such as the blue one, can reach the origin even when starting outside the ellipsoid.

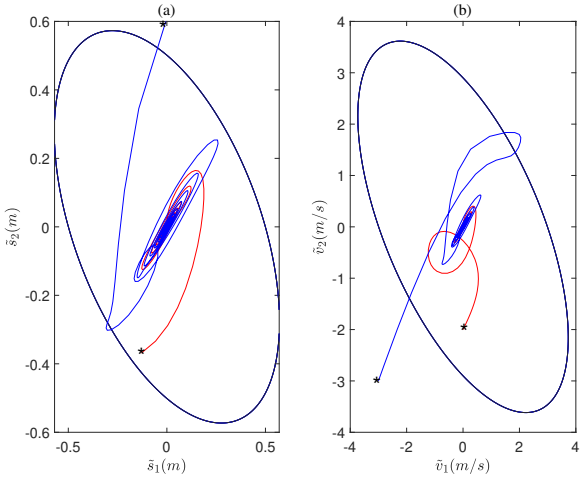

Fig. 3. Intersection of $\mathcal{S}(P,q)$ (black) with (a) $(\tilde{s}_1,\tilde{s}_2)$ plane, (b) $(\tilde{v}_1,\tilde{v}_2)$ plane, together with illustrative trajectories (starting points are represented by a star).

The maximum value of $\bar{z}$ that allows the LMI (21) to be feasible depends on various parameters of the model, including b and $v_{\max}$. Consequently, the volume of the optimal estimation of the ROA is also impacted by these parameters. In the followings, we investigate the effects of b and $v_{\max}$ on the volume of the optimal ellipsoidal estimation of the ROA around the origin, assuming that $d=d_0$. To achieve this, we determine the maximum-volume ellipsoidal estimation of ROA for different values of b and $v_{\max}$. We observe that decreasing b and increasing $v_{\max}$ result in a smaller maximum value of $\bar{z}$, which allows the LMI (21) to be feasible. This, in turn, leads to a smaller estimation of

TABLE I

DEPENDENCY OF THE ROA ESTIMATION ON b ($v_{\max} = 5\ m/s$).

$b\ [s^{-1}]$	Vector $\bar{z}$	Optimal volume of $\mathcal{S}(P,q)$
$b = 10$	$\bar{z}_i = 0.5601$	1.2×10^3
$b = 20$	$\bar{z}_i = 0.612$	3×10^9
$b = 30$	$\bar{z}_i = 0.702$	2.3×10^{11}

TABLE II

DEPENDENCY OF THE ROA ESTIMATION ON $v_{\max}$ ($b = 20\ s^{-1}$).

$v_{\max}\ [m/s]$	Vector $\bar{z}$	Optimal volume of $\mathcal{S}(P,q)$
$v_{\max} = 5$	$\bar{z}_i = 0.612$	3×10^9
$v_{\max} = 10$	$\bar{z}_i = 0.541$	1.4×10^5
$v_{\max} = 15$	$\bar{z}_i = 0.405$	101

ROA.

Specifically, by setting $v_{\max} = 5\ m/s$, we evaluate $\mathcal{S}(P,q)$ for various values of b. Our results, presented in Table I, reveal that increasing b results in a larger volume of the ROA estimation. We note that for each case with $\tilde{d} = d - d_0 = 0$, the maximum delays preserving the system's stability are determined based on Fig. 2. Moreover, as $d - d_0 = 0$, our analysis shows that the values of b must be larger than $5s^{-1}$, based on Fig. 2 (b).

Finally, we fix $b = 20\ s^{-1}$ and obtain the optimal estimation of ROA for different values of $v_{\max}$ by solving the optimization problem (35). We report the results in Table II, where we observe that increasing $v_{\max}$ leads to a decreasing volume of the ROA estimate. This implies that the trajectories of (14) reach the equilibrium for a smaller set of initial values.

V. CONCLUSION

This study utilizes the Optimal Velocity Model with driver reaction time to examine the collective dynamics of homogeneous vehicles on a ring-road. Incorporating a time-delay system enhances the model's accuracy in representing real-world traffic scenarios. The stability analysis of the equilibrium motion regime involves linearization, parameter analysis, and nonlinear estimation through LMIs. It highlights the importance of considering driver reaction time in the model and offers a nonlinear stability analysis for understanding vehicle collective behavior in traffic flow.

REFERENCES

[1] S. S. Mousavi and A. Kouvelas, "Structural observability of traffic density dynamics on a motorway ring road," in *IEEE Int. Conf. Intell. Transport. Syst.*, 2020, pp. 1–6.

[2] S. S. Avedisov, G. Bansal, and G. Orosz, "Impacts of connected automated vehicles on freeway traffic patterns at different penetration levels," *IEEE Trans. Intell. Transport. Syst.*, 2020.

[3] Y. Sugiyama, M. Fukui, M. Kikuchi, K. Hasebe, A. Nakayama, K. Nishinari, S.-i. Tadaki, and S. Yukawa, "Traffic jams without bottlenecks—experimental evidence for the physical mechanism of the formation of a jam," *New J. Phys.*, vol. 10, no. 3, p. 033001, 2008.

[4] M. R. Flynn, A. R. Kasimov, J.-C. Nave, R. R. Rosales, and B. Seibold, "Self-sustained nonlinear waves in traffic flow," *Phys. Rev. E*, vol. 79, no. 5, p. 056113, 2009.

[5] K. Nagel and M. Schreckenberg, "A cellular automaton model for freeway traffic," *J. Phys. I France*, vol. 2, no. 12, pp. 2221–2229, 1992.

[6] M. Bando, K. Hasebe, A. Nakayama, A. Shibata, and Y. Sugiyama, "Dynamical model of traffic congestion and numerical simulation," *Phys. Rev. E*, vol. 51, no. 2, p. 1035, 1995.

[7] S. S. Mousavi, S. Bahrami, and A. Kouvelas, "Controller design for a mixed traffic system travelling at different desired speeds," *Europ. J. Cont.*, vol. 68, p. 100698, 2022.

[8] S. S. Mousavi, S. Bahrami, and A. Kouvelas, "A gain-scheduled robust H_∞ control for a mixed traffic system travelling at different desired speeds in the presence of delay," in *IEEE Conf. Dec. Cont.*, 2022, pp. 1156–1161.

[9] S. S. Mousavi, S. Bahrami, and A. Kouvelas, "A mixed H_2/H_∞ controller design for a platoon with multiple human-driven and connected and automated vehicles," in *Europ. Cont. Conf.*, 2023, pp. 1–6.

[10] R. E. Stern, S. Cui, M. L. Delle Monache, R. Bhadani, M. Bunting, M. Churchill, N. Hamilton, H. Pohlmann, F. Wu, B. Piccoli, *et al.*, "Dissipation of stop-and-go waves via control of autonomous vehicles: Field experiments," *Transp. Res. Part C: Emerging Tech.*, vol. 89, pp. 205–221, 2018.

[11] S. Cui, B. Seibold, R. Stern, and D. B. Work, "Stabilizing traffic flow via a single autonomous vehicle: Possibilities and limitations," in *IEEE Intell. Vehicles Sympos.*, 2017, pp. 1336–1341.

[12] J. Wang, Y. Zheng, Q. Xu, J. Wang, and K. Li, "Controllability analysis and optimal control of mixed traffic flow with human-driven and autonomous vehicles," *IEEE Trans. Intell. Transport. Syst.*, 2020.

[13] S. S. Mousavi, S. Bahrami, and A. Kouvelas, "Output feedback controller design for a mixed traffic flow system moving in a loop," in *American Contr. Conf.*, 2021, pp. 192–197.

[14] S. S. Mousavi, S. Bahrami, and A. Kouvelas, "Synthesis of output-feedback controllers for mixed traffic systems in presence of disturbances and uncertainties," *IEEE Trans. Intell. Transport. Syst.*, vol. 24, no. 6, pp. 6450–6462, 2022.

[15] C. M. Gisolo, M. L. Delle Monache, F. Ferrante, and P. Frasca, "Nonlinear analysis of stability and safety of optimal velocity model vehicle groups on ring roads," *IEEE Trans. Intell. Transport. Syst.*, vol. 23, no. 11, pp. 20 628–20 635, 2022.

[16] S. S. Mousavi, S. Bahrami, and A. Kouvelas, "Expanding the boundaries of stability: Enlarging the region of attraction in mixed platoon systems," in *IEEE Intell. Transport. Syst.*, 2023.

[17] M. Bando, K. Hasebe, K. Nakanishi, and A. Nakayama, "Analysis of optimal velocity model with explicit delay," *Phys. Rev. E*, vol. 58, no. 5, p. 5429, 1998.

[18] L. Davis, "Modifications of the optimal velocity traffic model to include delay due to driver reaction time," *Phys. A: Stat. Mech. Applic.*, vol. 319, pp. 557–567, 2003.

[19] N. Olgac and R. Sipahi, "An exact method for the stability analysis of time-delayed linear time-invariant (lti) systems," *IEEE Trans. Automat. Contr.*, vol. 47, no. 5, pp. 793–797, 2002.

[20] R. M. Gray *et al.*, "Toeplitz and circulant matrices: A review," *Found. Trends® Commun. Info. Theory*, vol. 2, no. 3, pp. 155–239, 2006.

[21] K. Gu, J. Chen, and V. L. Kharitonov, *Stability of time-delay systems*. Springer Science & Business Media, 2003.

[22] X.-k. Xie, "Stable polynomials with complex coefficients," in *IEEE Conf. Dec. Contr.*, 1985, pp. 324–325.

[23] H. Yin, P. Seiler, and M. Arcak, "Stability analysis using quadratic constraints for systems with neural network controllers," *IEEE Transactions on Automatic Control*, vol. 67, no. 4, pp. 1980–1987, 2022.

[24] F. Zhang, *The Schur Complement and its Applications*. Springer Science and Business Media, 2006, vol. 4.

[25] H. Hindi and S. Boyd, "Analysis of linear systems with saturation using convex optimization," in *IEEE Conf. Dec. Cont.*, 1998, pp. 903–908.

[26] "Delay-dependent criteria for robust stability of time-varying delay systems," *Automatica*, vol. 40, no. 8, pp. 1435–1439, 2004.

[27] Y. Wang, L. Xie, and C. E. De Souza, "Robust control of a class of uncertain nonlinear systems," *Syst. & Cont. Lett.*, vol. 19, no. 2, pp. 139–149, 1992.